JLAB-THY-XX-XXXX

Pion Valence Quark Distribution at Large x from Lattice QCD

Raza Sabbir Sufian,[1] Colin Egerer,[2] Joseph Karpie,[3] Robert G. Edwards,[1] Bálint Joó,[1] Yan-Qing Ma,[4,5,6] Kostas Orginos,[1,2] Jian-Wei Qiu,[1] and David G. Richards[1]

[1] *Thomas Jefferson National Accelerator Facility, Newport News, VA 23606, USA*
[2] *Physics Department, William and Mary, Williamsburg, Virginia 23187, USA*
[3] *Physics Department, Columbia University, New York City, New York 10027, USA*
[4] *School of Physics and State Key Laboratory of Nuclear Physics and Technology, Peking University, Beijing 100871, China*
[5] *Center for High Energy physics, Peking University, Beijing100871, China*
[6] *Collaborative Innovation Center of Quantum Matter, Beijing 100871, China*

Using a short-distance collinear factorization, the pion valence quark distribution $q_v^\pi(x)$ is extracted from spacelike correlations of antisymmetrized vector and axial vector (V-A) currents, where the employed perturbative hard coefficient is derived to one-loop. Finite lattice spacing, volume, and quark mass dependencies are investigated in a simultaneous fit of matrix elements computed on four gauge ensembles, providing a physical limit Ioffe time distribution. Using two different phenomenologically motivated parametrizations of $q_v^\pi(x)$, the $q_v^\pi(x)$ distribution is found to be in very good agreement with that extracted from experimental data. At large x, a softer valence quark distribution is slightly favored by the figure of merit of this calculation. These two distributions are consistent within uncertainty and reproduce the extraction of $q_v^\pi(x)$ from the experimental data in the entire x-region, showing the robustness of our calculation.

Introduction: The pion, being both a Nambu-Goldstone boson and the lightest bound state in Quantum Chromo-Dynamics (QCD), highlights the challenges in creating consistent theoretical and phenomenological frameworks to describe its partonic structure. The shape of the pion valence parton distribution functions (PDFs) extracted from experimental data [1–5] in different analyses [6–12] are in sharp contrast among themselves and with perturbative QCD (pQCD)-based frameworks [13, 14] at large longitudinal momentum fractions x. Central to the disparity is whether the pion PDF has a softer (harder) $(1-x)^2$ ($(1-x)$) fall-off as $x \to 1$, and at what x and Q^2 pQCD predictions are matched - various model calculations [15–20] exemplify this contrast.

The limited available phase space for partonic interactions at large x localizes quantum fluctuations such that large-x dynamics is constrained by confinement, in effect increasing parton correlations as $x \to 1$. As the quark distribution at large x is sensitive to non-perturbative quark-gluon dressing, a description of its behavior will also elucidate our understanding of the generation of mass in QCD through dynamical chiral symmetry breaking. Unraveling the complexities of the valence and sea quark contents of the pion is spearheaded by several upcoming experiments - Jefferson Lab tagged deep-inelastic scattering (DIS) experiments [21], Drell-Yan measurements at the COMPASS experiment [22] and, also the future Electron-Ion Collider (EIC) facility [23]. A first-principles lattice QCD (LQCD) determination of the pion valence PDF $q_v^\pi(x)$ with controlled statistical and systematic uncertainties is particularly well-timed and solicits a synergy of increasing importance between experimental and theoretical efforts.

Experimental extraction of x-dependent parton physics has blossomed through the application of the QCD factorization theorem [24] and considerable advancements in global analyses [25–29] of experimental data. Besides, several LQCD methods [30–36] have been proposed and developed that probe the light-cone structure of hadrons non-perturbatively. These approaches have led to significant achievements in recent years, especially in determinations of flavor non-singlet distributions [37–45]. A proper quantification and mitigation of systematic errors and numerical artifacts present in these calculations and related theoretical challenges still require further insight and development (for a recent review, see [46]). Incorporating LQCD calculated quantities as a component of future global analyses remains a goal of the pQCD and LQCD communities providing further impetus to overcome these challenges.

In this letter, we present a calculation of the $q_v^\pi(x)$ obtained from "Lattice Cross Sections" (LCSs) [34, 36], specifically matrix elements of two local, spacelike-separated, gauge-invariant currents within the pion. The Lorentz covariant matrix elements of two currents spatially separated by a quark propagator are computable on a Euclidean lattice and have a well-defined continuum limit as the lattice spacing $a \to 0$. In our calculation, through the factorization of these hadronic matrix elements, the collinear divergences of the partonic scattering are absorbed into the non-perturbative PDFs, leaving an infrared-safe and perturbatively computable hard contribution, in direct analogy to the factorization of inclusive DIS cross sections measurements in experiments. Calculations on four distinct lattice ensembles allows for estimating systematic errors from finite lattice spacing, volume, and unphysical pion mass extrapolations. These results are shown following a derivation of the next-to-leading-order (NLO) perturbative kernel for an antisymmetrized vector-axial (V-A) current combina-

tion and contact is made with parton densities in a manner akin a global analysis of experimental observables.

Next-to-leading order perturbative kernel: Following our previous work [41], we consider the following matrix element in a hadron h

$$\sigma_{VA}^{h,\mu\nu}(\xi,p) = \xi^4 Z_V Z_A \langle h(p)| T\{[\overline{\psi}\gamma^\mu\psi](\xi) [\overline{\psi}\gamma^\nu\gamma^5\psi](0)\} |h(p)\rangle , \quad (1)$$

where $\sigma_{VA}^{h,\mu\nu}$ depends covariantly on the hadron momentum p and spatial separation ξ between the currents; $Z_{V,A}$ are the renormalization constants of the local currents determined in [47] for the ensembles used in this calculation. A Lorentz decomposition of Eq. (1) yields structures σ_{VA}^h that depend on the invariant spacelike interval between currents and the Ioffe time [48], $\omega = p\cdot\xi$, of the process. As a result of the invariance of strong interaction under parity and time reversal transformations $\sigma_{VA}^h(\omega,\xi^2,p^2) = -\sigma_{VA}^h(-\omega,\xi^2,p^2)$ and we have the factorization relation [36]

$$\sigma_{VA}^h(\omega,\xi^2,p^2) = \sum_q \int_0^1 \frac{dx}{x} K(x\omega,\xi^2,x^2p^2,\mu^2) \times f_{q_v/h}(x,\mu^2) + \mathcal{O}(\xi^2\Lambda_{\rm QCD}^2), \quad (2)$$

where the perturbative kernel has the property $K(x\omega,\xi^2,x^2p^2,\mu^2) = -K(-x\omega,\xi^2,x^2p^2,\mu^2)$, μ^2 is the factorization scale, and $f_{q_v/h}(x,\mu^2) \equiv f_{q/h}(x,\mu^2) - f_{\overline{q}/h}(x,\mu^2)$ are valence PDFs. As $K(x\omega,\xi^2,x^2p^2,\mu^2)$ depends on the coordinate-space variable ξ, it is difficult to apply conventional perturbative calculation techniques, developed usually for momentum-space calculations. A rigorous derivation of this hard part in both coordinate and momentum space, and critical need for keeping ξ small will be presented in an upcoming calculation [49]. To perturbatively calculate $K(x\omega,\xi^2,0,\mu^2)$, we define the momentum-space LCS

$$\widetilde{\sigma}_{VA}^h(\widetilde{\omega},q^2) \equiv \int \frac{d^D\xi}{\xi^4} e^{iq\cdot\xi}\, \sigma_{VA}^h(\omega,\xi^2,0) = \int_0^1 \frac{dx}{x} \widetilde{K}(x\widetilde{\omega},q^2,\mu^2) f_{q_v/h}(x,\mu^2) + \mathcal{O}(\Lambda_{\rm QCD}^2/q^2), \quad (3)$$

where $D = 4-2\epsilon$ is the space-time dimension, $\widetilde{\omega} = \frac{2p\cdot q}{-q^2-i0^+}$ and a momentum space factorization of $\widetilde{\sigma}_{VA}^h(\widetilde{\omega},q^2)$ has been performed. K is obtained from $\widetilde{K}$:

$$K(x\omega,\xi^2,0,\mu^2) = \xi^4 \int \frac{d^Dq}{(2\pi)^D} e^{-iq\cdot\xi} \widetilde{K}(x\widetilde{\omega},q^2,\mu^2) . \quad (4)$$

To calculate $\widetilde{K}$, we project h onto a parton state q in Eq. (3) and expand both sides in powers of the strong coupling α_s, *i.e.* $\widetilde{K} = \widetilde{K}^{(0)} + \alpha_s\widetilde{K}^{(1)} + \cdots$, and similarly for $f_{q_v/q}$, which up to first order in α_s results in

$$\widetilde{\sigma}_{VA}^{q(0)}(\widetilde{\omega},q^2) = \int_0^1 \frac{dx}{x} \widetilde{K}^{(0)}(x\widetilde{\omega},q^2,\mu^2) f_{q_v/q}^{(0)}(x,\mu^2), \quad (5a)$$

$$\widetilde{\sigma}_{VA}^{q(1)}(\widetilde{\omega},q^2) = \int_0^1 \frac{dx}{x} \widetilde{K}^{(1)}(x\widetilde{\omega},q^2,\mu^2) f_{q_v/q}^{(0)}(x,\mu^2) + \int_0^1 \frac{dx}{x} \widetilde{K}^{(0)}(x\widetilde{\omega},q^2,\mu^2) f_{q_v/q}^{(1)}(x,\mu^2). \quad (5b)$$

The perturbative expansion of renormalized PDFs is well-known,

$$f_{q_v/q}^{(0)}(x,\mu^2) = \delta(1-x), \quad (6a)$$

$$f_{q_v/q}^{(1)}(x,\mu^2) = -\frac{1}{\epsilon}\frac{(4\pi)^\epsilon}{\Gamma(1-\epsilon)}\frac{\alpha_s}{2\pi} C_F \left(\frac{1+x^2}{1-x}\right)_+ , \quad (6b)$$

where we choose the $\overline{\rm MS}$ renormalization scheme. Based on Eqs. (5) and (6), $\widetilde{K}^{(0)}$ and $\widetilde{K}^{(1)}$ are fully determined by $\widetilde{\sigma}_{VA}^{q(0)}$ and $\widetilde{\sigma}_{VA}^{q(1)}$. The calculation of $\widetilde{\sigma}_{VA}^{q(0)}$ and $\widetilde{\sigma}_{VA}^{q(1)}$ up to $\mathcal{O}(\alpha_s)$ can be obtained from the lowest order and one-loop Feynman diagrams. Due to Ward-Takahashi identities for vector current and axial-vector current, UV divergences cancel out within one-loop diagrams and we do not need perturbative renormalization, which means $Z_V = Z_A = 1$ in the perturbative calculation. One can also verify that perturbative collinear divergences from $\widetilde{\sigma}_{VA}^{q(1)}$ cancel exactly with $f_{q_v/q}^{(1)}$ in Eq. (5), resulting in finite $\widetilde{K}^{(0)}$ and $\widetilde{K}^{(1)}$, and thus up to $\mathcal{O}(\alpha_s)$

$$\widetilde{K}^{\mu\nu}(\widetilde{\omega},q^2,\mu^2) = \frac{\epsilon^{\mu\nu\alpha\beta}q_\alpha p_\beta}{p\cdot q}\Bigg\{\frac{1}{1+\widetilde{\omega}} + \frac{\alpha_s C_F}{4\pi} \times \Bigg[\left(\frac{2+2\widetilde{\omega}^2}{\widetilde{\omega}+\widetilde{\omega}^2}\ln(1+\widetilde{\omega}) + \frac{3\widetilde{\omega}}{1-\widetilde{\omega}^2}\right)\ln\left(\frac{\mu^2}{-q^2-i0^+}\right) + \frac{5\widetilde{\omega}}{1-\widetilde{\omega}^2} + \frac{2-2\widetilde{\omega}-\widetilde{\omega}^2}{\widetilde{\omega}+\widetilde{\omega}^2}\ln(1+\widetilde{\omega}) - \frac{1+\widetilde{\omega}^2}{\widetilde{\omega}+\widetilde{\omega}^2}\ln^2(1+\widetilde{\omega})\Bigg]\Bigg\} - (\widetilde{\omega}\to-\widetilde{\omega}). \quad (7)$$

By performing a Fourier transform, we obtain

$$K^{\mu\nu}(\omega,\xi^2,\mu^2) = \frac{1}{\pi^2}\frac{\epsilon^{\mu\nu\alpha\beta}\xi_\alpha p_\beta}{p\cdot\xi}[K^{(0)}(\omega) + \frac{\alpha_s C_{\rm F}}{2\pi} \{K^{(1,0)}(\omega) + K^{(1,1)}(\omega)\ln(-\xi^2\mu^2 e^{2\gamma_E}/4)\}], \quad (8)$$

with

$$K^{(0)}(\omega) = 2\omega\cos\omega, \quad (9)$$

$$K^{(1,0)}(\omega) = 2\omega\int_0^1 dy\cos(y\omega)\left[\frac{1}{2}\delta(1-y) - \left(\frac{2\ln(1-y)}{1-y} - \frac{y^2-3y+1}{1-y}\right)_+\right]$$

$$K^{(1,1)}(\omega) = -2\omega\int_0^1 dy\cos(y\omega)\left(\frac{1+y^2}{1-y}\right)_+ , \quad (10)$$

where the leading order kernel $K^{(0)}(\omega)$ in Eq. (9) is the same as the result in [41]. It is crucial to mention that a large p alone does not guarantee the applicability of

ID	a (fm)	m_π (MeV)	$L^3 \times N_t$	$N_{\rm cfg}$
$a127m413$	0.127(2)	413(4)	$24^3 \times 64$	2124
$a127m413L$	0.127(2)	413(5)	$32^3 \times 96$	490
$a94m358$	0.094(1)	358(3)	$32^3 \times 64$	417
$a94m278$	0.094(1)	278(4)	$32^3 \times 64$	503

TABLE I. Parameters for each gauge ensemble used in this work: lattice spacing, pion mass, spatial and temporal sizes, and number of configurations used.

perturbative expansion and contributions from large ξ can invalidate the perturbative factorization [36, 41].

Numerical Results & Extraction of the $q_v^\pi(x)$: This calculation is carried out on four different 2+1 flavor QCD ensembles (listed in Table I) using the isotropic-clover fermion action generated by the JLab/W&M Collaboration [50]. We refer to [41] for details about the implementation of a modified sequential source technique, and a combination of Jacobi and momentum smearing to obtain matrix elements for a given momentum p and spatial separation ξ between the currents. In this calculation of the forward matrix elements, the pion source-sink separation T is systematically increased, while holding fixed the current insertion time $t = T/2$, ensuring identical excited-state contamination from both source and sink sides. To extract the desired matrix elements, we assume the following forms of two- and four-point correlation functions:

$$C_{2pt}(T) = A\, e^{-m_0 T}$$
$$C_{4pt}(T) = e^{-m_0 T}(B + D\, e^{-\Delta m T}), \qquad (11)$$

and perform simultaneous correlated fits to the two- and four-point functions. We verify that the value of ground-state energy m_0 obtained from this simultaneous fit is consistent with that obtained from $C_{2pt}(T)$ alone and also agrees with the energy-momentum dispersion relation.

In FIG. 1, we present fit results of the ratio $C_{4pt}(T)/e^{-m_0 T}$ on the ensembles $a94m278$ and $a94m358$ for momenta in the range $p \in \{0.41 - 1.65\}$ GeV and current separation $\xi = 3a$, both p and ξ in along the z-direction, to demonstrate how reliably we can extract the asymptotic value of B, and hence the Ioffe time distribution from B/A. The numerical challenges manifest in this formalism are reflected in the signal-to-noise ratio (S/N) of the largest momentum $p = 1.65$ GeV relative to that of the smallest $p = 0.41$ GeV; the former is nearly 3 times smaller. Despite this, we can fit these data up to at least $T = 14(\sim 1.32$ fm) even for the largest momentum $p = 1.65$ GeV on the lightest pion mass $m_\pi = 278$ MeV ensemble. In all the fits, we use the time window such that $S/N \geq 1$. Moreover, the $\xi = a$ matrix elements are affected by the contact terms arising from the clover term connecting neighboring lattice sites and the matrix element deviates significantly from other data points. We exclude these matrix elements in our analysis.

The matrix elements computed across the four gauge ensembles are shown in FIG. 2. We only include $|\xi| \leq$

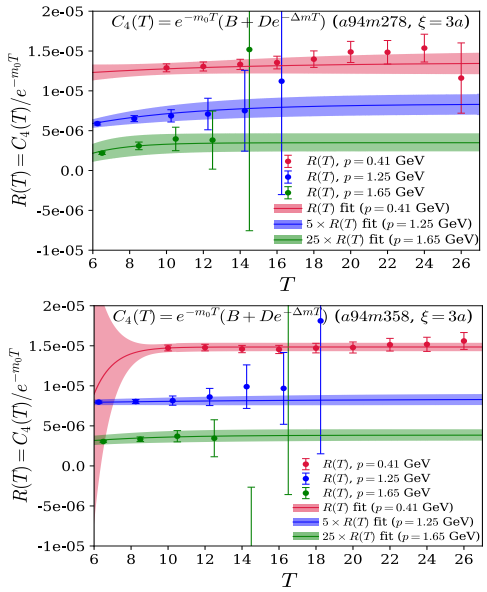

FIG. 1. Removal of the leading ground-state time dependence exposes the desired matrix elements in the large T limit, shown here for ensembles $a94m278$ (above) and $a94m358$ (below) for current separations $\xi = 3a$. High momenta data rescaled for S/N comparison.

0.56 fm in our analysis so that ξ is sufficiently smaller than $\Lambda_{\rm QCD}^{-1}$, thereby ensuring the validity of the short-distance factorization and minimizing higher-twist contributions from large ξ. Exploiting the analyticity of the

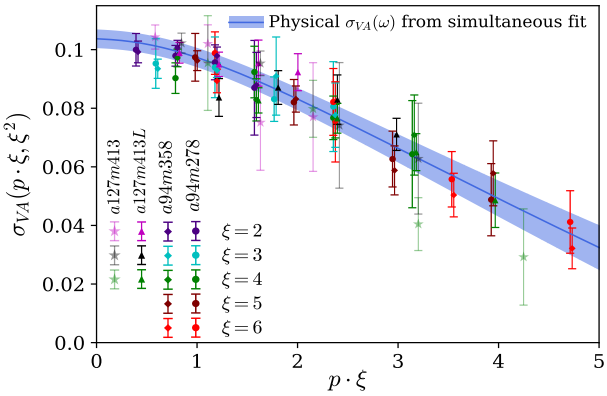

FIG. 2. Simultaneous fit to the antisymmetric V-A currents matrix element on four different ensembles. The blue band indicates the Ioffe time distribution in the physical limit.

LCS $\sigma_{VA}(\omega \equiv p \cdot \xi, \xi^2)$ in ω, we obtain the Ioffe time distribution using a flexible z-expansion fit [51, 52] supplemented with chiral, continuum, finite volume [53] and higher twist corrections:

$$\sigma_{VA}(\omega, \xi^2) = \sum_{k=0}^{k_{\rm max}=4} \lambda_k \tau^k + b_1 m_\pi + b_2 a + b_3 \xi^2 + b_4 a^2 p^2 + b_5 e^{-m_\pi (L-\xi)}, \qquad (12)$$

$$\text{where} \quad \tau = \frac{\sqrt{\omega_{\rm cut} + \omega} - \sqrt{\omega_{\rm cut}}}{\sqrt{\omega_{\rm cut} + \omega} + \sqrt{\omega_{\rm cut}}}. \qquad (13)$$

Inclusion of higher-order terms beyond $k_{\max} = 4$ have no statistical significance and are not considered in the z-expansion fit (12). We choose $\omega_{\rm cut} = 1.0$ as used in [54]; other choices of $\omega_{\rm cut}$ were observed to have no effect on the final band in the physical limit and vanishing contribution of $\mathcal{O}(\xi^2)$ higher twist effect (FIG. 2) where b_i corrections of Eq. (12) have been implemented. The fit yields

$$\begin{aligned}&\lambda_0 = 0.104(3),\ \lambda_1 = -0.006(3),\ \lambda_2 = -0.029(9),\\ &\lambda_3 = -0.943(404),\ \lambda_4 = 0.124(136),\\ &b_1 = 0.174(96),\ b_2 = -0.083(43),\ b_3 = -0.0004(7),\\ &b_4 = 0.007(8),\ b_5 = 0.102(51)\end{aligned} \tag{14}$$

with $\chi^2/\text{d.o.f} = 1.20$. With the physical $\sigma_{VA}(\omega)$ distribution in hand, we can immediately extract the physical $q_{\rm v}^\pi(x)$ with no further extrapolations.

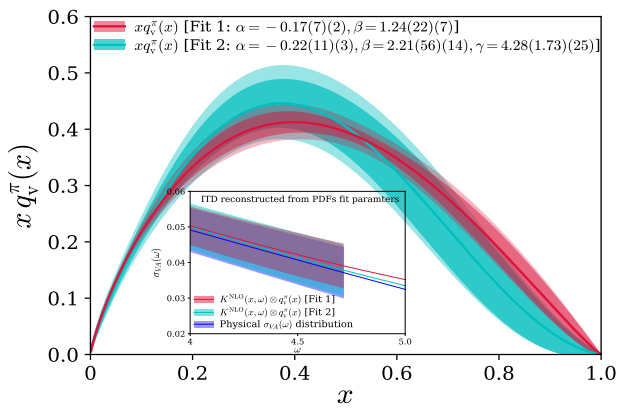

FIG. 3. The pion valence quark distribution obtained from fitting the convolution of $q_{\rm v}^\pi(x)$ and the NLO perturbative kernel (8) to the determined $\sigma_{VA}(\omega)$ distribution in the fit Eq. (12). Fits 1 and 2 label the 2- and 3-parameter functional forms in Eq. (15). [Inset] A comparison of the reconstructed $\sigma_{VA}(\omega)$-distribution for $4.0 < \omega < 5.0$ from the PDF fits and that obtained from (12).

The extraction of $q_{\rm v}^\pi(x)$ is achieved by numerically evaluating the convolution of the NLO kernel (Eq. (8)) and two phenomenologically motivated functional forms of the PDF:

$$q_{\rm v}^\pi(x) = \frac{x^\alpha(1-x)^\beta(1+\gamma x)}{B(\alpha+1,\beta+1)+\gamma B(\alpha+2,\beta+1)} \tag{15}$$

and fit the $\sigma_{VA}(\omega)$ distribution using the numerical fitting program ROOT [55]. We use the strong coupling $\alpha_s = 0.303$ at the initial scale $\mu_0 = 2$ GeV [56]. The systematic uncertainties in the PDF fit parameters are estimated by a 10% variation in α_s as in [54]. The 2-parameter fit, by fixing $\gamma = 0$ in Eq. (15) yields,

$$\alpha = -0.17(7)_{\rm stat}(2)_{\rm sys}, \quad \beta = 1.24(22)_{\rm stat}(7)_{\rm sys} \tag{16}$$

with $\chi^2/\text{d.o.f} = 1.41$. Stated uncertainties are statistical (systematic) first (second). In a 3-parameter fit, with an uncontrained γ, we obtain

$$\begin{aligned}&\alpha = -0.22(11)_{\rm stat}(3)_{\rm sys},\ \beta = 2.12(56)_{\rm stat}(14)_{\rm sys},\\ &\gamma = 4.28(1.73)_{\rm stat}(25)_{\rm stat}\end{aligned} \tag{17}$$

with $\chi^2/\text{d.o.f} \approx 1.29$. Inclusion of an additional $\rho\sqrt{x}$-term in (15) was found to be consistent with zero. Commensurate $\chi^2/\text{d.o.f}$ between fits (16) and (17) limits the selection of one fit over another based solely on the goodness of the fit. However, the fit (17) includes the possibility of $\gamma = 0$ and is more general. These fits are shown in FIG. 3. We elected not to extrapolate our Ioffe time distribution obtained from our z-expansion fit beyond the largest Ioffe time $\omega = 4.71$ when determining the PDF. However for illustration purposes (FIG. 3 inset), extrapolating the central value of the $\sigma_{VA}(\omega)$ distribution from the z-expansion fit (blue) and the associated 2- (red) and 3-parameter (cyan) fits reveals that precise LQCD data at large-ω are required to distinguish between different large-x behaviors of $q_{\rm v}^\pi(x)$. We find the $\sigma_{VA}(\omega)$-distribution reconstructed from the 2-parameter fit slightly underestimates the uncertainties of the distribution in the physical limit. This observation together with the smaller $\chi^2/\text{d.o.f}$ favors the $q_{\rm v}^\pi(x)$ extracted using the 3-parameter fit (17).

Discussion: For a comparison with global fits of $q_{\rm v}^\pi(x)$, we evolve our extracted PDF sets to a scale of $\mu^2 = 27$ GeV^2, from an initial scale $\mu_0 = 2$ GeV shown in FIG. 3, large enough for the validity of factorization. FIG. 4 shows a comparison with the PDF extraction using LO factorization of the E615 data [3], which shows a $(1-x)$ large-x behavior, and the analysis [11] where the next-to-leading-logarithmic threshold soft-gluon re-summation effects [57, 58] are included in the calculation of the Drell-Yan cross section, which shows a softer $(1-x)^2$ fall-off. Notably, in a NLO analysis of the E615 data [10], the large-x behavior was found to be $\sim (1-x)^{1.54}$. Following the discussion in the previous section, we note from FIG. 4 that our more flexible fit (17), with smaller $\chi^2/\text{d.o.f}$, has good agreement with the analysis in [11] over the entire x-region.

When compared to previous LQCD calculations of $q_{\rm v}^\pi(x)$, the present calculation shows good agreement with the previous LCSs calculation [41] and $q_{\rm v}^\pi(x)$ obtained in [54] using the "reduced pseudo Ioffe time distribution" formalism [35]; although $q_{\rm v}^\pi(x, \mu^2 = 27\,\text{GeV}^2)$ in [54] shows some tension with the E615 data in the $0.42 < x < 0.8$ region. Corresponding calculations using the "quasi-PDFs" formalism [33] show differences among themselves and in $0.4 < x < 0.85$ region in [60] and in $x > 0.62$ region in [43] with our calculation and the experimental extraction of $q_{\rm v}^\pi(x)$.

Conclusion & Outlook: This work presents the first calculation of LCS that incorporates results on four gauge ensembles, including the lightest pion mass used in any lattice QCD calculation to access $q_{\rm v}^\pi(x)$, along with a derivation of the one-loop perturbative matching kernel for the antisymmetric vector-axial current combination. The resultant PDFs obtained are in agreement

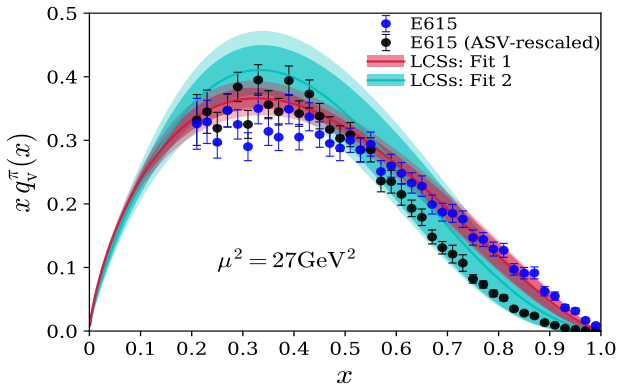

FIG. 4. Comparison of pion $xq_v^\pi(x)$-distribution obtained from this calculation with the $xq_v^\pi(x)$ distributions extracted from the experimental Drell-Yan cross sections. The blue data points are from LO analysis [3] and the "ASV-rescaled" black data points compiled from [59] are the E615 re-scaled data according to analysis [11].

with the $q_v^\pi(x)$ extracted from the experimental data. From our analysis, we have the indication that a $(1-x)^2$-behavior of the $q_v^\pi(x)$ at large x is preferred. Future calculation with finer lattice spacings and access to larger momentum, thus providing data at higher Ioffe time ($\omega \sim 8-10$) will provide further clarification to distinguish between the softer $(1-x)^2$ and harder $(1-x)$ fall-off of the $q_v^\pi(x)$-distribution that can complement experiment and resolve the large-x behavior. The simpler non-perturbative UV renormalization of the current-current operators, the availability of current combinations, and the remarkable agreement of this result with the experimentally extracted $q_v^\pi(x)$ in the entire x-region demonstrate the potential of this method to unravel the enigmatic structure of the pion.

Acknowledgments: We thank Carl Carlson, Martha Constantinou, Luka Leskovec, Tianbo Liu, Wayne Morris, Anatoly Radyushkin, Nobuo Sato, and Jian-Hui Zhang who provided insights and expertise that greatly assisted this research.

This work is supported by Jefferson Science Associates, LLC under U.S. DOE Contract #DE-AC05-06OR23177 within the framework of the TMD Collaboration. We acknowledge the facilities of the USQCD Collaboration used for this research in part, which are funded by the Office of Science of the U.S. Department of Energy. This material is based in part upon work supported by a grant from the Southeastern Universities Research Association (SURA) under an appropriation from the Commonwealth of Virginia. This work used the Extreme Science and Engineering Discovery Environment (XSEDE), which is supported by National Science Foundation grant number ACI-1548562 [61], and the Texas Advanced Computing Center (TACC) at the University of Texas at Austin for providing HPC resources on `Frontera` that have contributed to the results in this paper. This work was performed in part using computing facilities at William and Mary which were provided by contributions from the National Science Foundation (MRI grant PHY-1626177), the Commonwealth of Virginia Equipment Trust Fund and the Office of Naval Research. In addition, this work used resources at NERSC, a DOE Office of Science User Facility supported by the Office of Science of the U.S. Department of Energy under Contract #DE-AC02-05CH11231, as well as resources of the Oak Ridge Leadership Computing Facility at the Oak Ridge National Laboratory, which is supported by the Office of Science of the U.S. Department of Energy under Contract No. #DE-AC05-00OR22725. The software codes `Chroma` [62], `QUDA` [63, 64] and `QPhiX` [65] were used. The authors acknowledge support from the U.S. Department of Energy, Office of Science, Office of Advanced Scientific Computing Research and Office of Nuclear Physics, Scientific Discovery through Advanced Computing (SciDAC) program. Also acknowledged is support from the U.S. Department of Energy Exascale Computing Project. C.E. is supported in part by the U.S. Department of Energy under contract DE-FG02-04ER41302 and a Department of Energy Office of Science Graduate Student Research fellowship, through the U.S. Department of Energy, Office of Science, Office of Workforce Development for Teachers and Scientists, Office of Science Graduate Student Research (SCGSR) program. Y. M. is supported in part by the National Natural Science Foundation of China under Grant Numbers 11875071 and 11975029. K.O. acknowledges support in part by the U.S. Department of Energy through Grant Number DE- FG02-04ER41302, by STFC consolidated grant ST/P000681/1.

[1] J. Badier *et al.* [NA3 Collaboration], "Experimental Determination of the pi Meson Structure Functions by the Drell-Yan Mechanism," Z. Phys. C **18**, 281 (1983).

[2] B. Betev *et al.* [NA10 Collaboration], "Differential Cross-section of High Mass Muon Pairs Produced by a 194-GeV/$c\pi^-$ Beam on a Tungsten Target," Z. Phys. C **28**, 9 (1985).

[3] J. S. Conway *et al.*, "Experimental Study of Muon Pairs Produced by 252-GeV Pions on Tungsten," Phys. Rev. D **39**, 92 (1989).

[4] S. Chekanov *et al.* [ZEUS Collaboration], "Leading neutron production in e+ p collisions at HERA," Nucl. Phys. B **637**, 3 (2002).

[5] F. D. Aaron *et al.* [H1 Collaboration], "Measurement of Leading Neutron Production in Deep-Inelastic Scattering at HERA," Eur. Phys. J. C **68**, 381 (2010).

[6] J. F. Owens, "Q^2 Dependent Parametrizations of Pion Parton Distribution Functions," Phys. Rev. D **30**, 943 (1984).

[7] P. Aurenche, R. Baier, M. Fontannaz,

M. N. Kienzle-Focacci and M. Werlen, "The Gluon Content of the Pion From High p_T Direct Photon Production," Phys. Lett. B **233**, 517 (1989).

[8] P. J. Sutton, A. D. Martin, R. G. Roberts and W. J. Stirling, "Parton distributions for the pion extracted from Drell-Yan and prompt photon experiments," Phys. Rev. D **45**, 2349 (1992).

[9] M. Gluck, E. Reya and A. Vogt, "Pionic parton distributions," Z. Phys. C **53**, 651 (1992).

[10] K. Wijesooriya, P. E. Reimer and R. J. Holt, "The pion parton distribution function in the valence region," Phys. Rev. C **72**, 065203 (2005).

[11] M. Aicher, A. Schafer and W. Vogelsang, "Soft-gluon resummation and the valence parton distribution function of the pion," Phys. Rev. Lett. **105**, 252003 (2010).

[12] P. C. Barry, N. Sato, W. Melnitchouk and C. R. Ji, "First Monte Carlo Global QCD Analysis of Pion Parton Distributions," Phys. Rev. Lett. **121**, no. 15, 152001 (2018).

[13] G. R. Farrar and D. R. Jackson, "The Pion Form-Factor," Phys. Rev. Lett. **43**, 246 (1979).

[14] E. L. Berger and S. J. Brodsky, "Quark Structure Functions of Mesons and the Drell-Yan Process," Phys. Rev. Lett. **42**, 940 (1979).

[15] T. Shigetani, K. Suzuki and H. Toki, "Pion structure function in the Nambu and Jona-Lasinio model," Phys. Lett. B **308**, 383 (1993).

[16] R. M. Davidson and E. Ruiz Arriola, "Structure functions of pseudoscalar mesons in the SU(3) NJL model," Phys. Lett. B **348**, 163 (1995).

[17] M. B. Hecht, C. D. Roberts and S. M. Schmidt, "Valence quark distributions in the pion," Phys. Rev. C **63**, 025213 (2001).

[18] C. Chen, L. Chang, C. D. Roberts, S. Wan and H. S. Zong, "Valence-quark distribution functions in the kaon and pion," Phys. Rev. D **93**, 074021 (2016).

[19] G. F. de Téramond, T. Liu, R. S. Sufian, H. G. Dosch, S. J. Brodsky and A. Deur[HLFHS Collaboration], "Universality of Generalized Parton Distributions in Light-Front Holographic QCD," Phys. Rev. Lett. **120**, no. 18, 182001 (2018).

[20] K. D. Bednar, I. C. Cloët and P. C. Tandy, "Distinguishing Quarks and Gluons in Pion and Kaon PDFs," `arXiv:1811.12310 [nucl-th]`.

[21] Dasuni Adikaram, *et al.*, Hall A and SBS Collaboration Proposal, "Measurement of Tagged Deep Inelastic Scattering (TDIS)," PR12-15-006.

[22] B. Adams *et al.*, "Letter of Intent: A New QCD facility at the M2 beam line of the CERN SPS (COMPASS++/AMBER)," `arXiv:1808.00848 [hep-ex]`.

[23] A. C. Aguilar *et al.*, "Pion and Kaon Structure at the Electron-Ion Collider," Eur. Phys. J. A **55**, no. 10, 190 (2019).

[24] J. C. Collins, D. E. Soper and G. F. Sterman, "Factorization of Hard Processes in QCD," Adv. Ser. Direct. High Energy Phys. **5**, 1 (1989).

[25] L. A. Harland-Lang, A. D. Martin, P. Motylinski and R. S. Thorne, "Parton distributions in the LHC era: MMHT 2014 PDFs," Eur. Phys. J. C **75**, 204 (2015).

[26] S. Dulat *et al.*, "New parton distribution functions from a global analysis of quantum chromodynamics," Phys. Rev. D **93**, 033006 (2016).

[27] R. D. Ball *et al.* (NNPDF Collaboration), "Parton distributions from high-precision collider data," Eur. Phys. J. C **77**, 663 (2017).

[28] S. Alekhin, J. Blümlein, S. Moch and R. Plačakytė, "Parton distribution functions, α_s, and heavy-quark masses for LHC Run II," Phys. Rev. D **96**, 014011 (2017).

[29] J. J. Ethier, N. Sato and W. Melnitchouk, "First simultaneous extraction of spin-dependent parton distributions and fragmentation functions from a global QCD analysis," Phys. Rev. Lett. **119**, no. 13, 132001 (2017).

[30] K. F. Liu and S. J. Dong, "Origin of difference between $\overline{d}$ and $\overline{u}$ partons in the nucleon," Phys. Rev. Lett. **72**, 1790 (1994).

[31] V. Braun and D. Mueller, "Exclusive processes in position space and the pion distribution amplitude," Eur. Phys. J. C **55**, 349 (2008).

[32] R. Horsley *et al.* (QCDSF-UKQCD Collaboration), "A lattice study of the glue in the nucleon," Phys. Lett. B **714**, 312 (2012).

[33] X. Ji, "Parton physics on a Euclidean lattice," Phys. Rev. Lett. **110**, 262002 (2013).

[34] Y. Q. Ma and J. W. Qiu, "Extracting Parton Distribution Functions from Lattice QCD Calculations," Phys. Rev. D **98**, no. 7, 074021 (2018).

[35] A. V. Radyushkin, "Quasi-parton distribution functions, momentum distributions, and pseudo-parton distribution functions," Phys. Rev. D **96**, 034025 (2017).

[36] Y. Q. Ma and J. W. Qiu, "Exploring Partonic Structure of Hadrons Using ab initio Lattice QCD Calculations," Phys. Rev. Lett. **120**, no. 2, 022003 (2018).

[37] A. J. Chambers *et al.*, "Nucleon structure functions from operator product expansion on the lattice," Phys. Rev. Lett. **118**, 242001 (2017).

[38] C. Alexandrou, K. Cichy, M. Constantinou, K. Jansen, A. Scapellato and F. Steffens, "Light-Cone Parton Distribution Functions from Lattice QCD," Phys. Rev. Lett. **121**, no. 11, 112001 (2018).

[39] G. S. Bali *et al.*, "Pion distribution amplitude from Euclidean correlation functions: Exploring universality and higher-twist effects," Phys. Rev. D **98**, no. 9, 094507 (2018).

[40] H. W. Lin *et al.*, "Proton Isovector Helicity Distribution on the Lattice at Physical Pion Mass," Phys. Rev. Lett. **121**, no. 24, 242003 (2018).

[41] R. S. Sufian, J. Karpie, C. Egerer, K. Orginos, J. W. Qiu and D. G. Richards, "Pion Valence Quark Distribution from Matrix Element Calculated in Lattice QCD," Phys. Rev. D **99**, no. 7, 074507 (2019).

[42] G. S. Bali *et al.* [RQCD Collaboration], "Light-cone distribution amplitudes of octet baryons from lattice QCD," Eur. Phys. J. A **55**, no. 7, 116 (2019).

[43] T. Izubuchi, L. Jin, C. Kallidonis, N. Karthik, S. Mukherjee, P. Petreczky, C. Shugert and S. Syritsyn, "Valence parton distribution function of pion from fine lattice," Phys. Rev. D **100**, no. 3, 034516 (2019).

[44] J. Liang *et al.* [χQCD Collaboration], "Towards the nucleon hadronic tensor from lattice QCD," `arXiv:1906.05312 [hep-ph]`.

[45] B. Joó, J. Karpie, K. Orginos, A. Radyushkin, D. Richards and S. Zafeiropoulos, "Parton Distribution Functions from Ioffe time pseudo-distributions," JHEP **1912**, 081 (2019).

[46] K. Cichy and M. Constantinou, "A guide to light-cone PDFs from Lattice QCD: an overview of approaches, techniques and results," Adv. High Energy Phys. **2019**, 3036904 (2019).

[47] B. Yoon *et al.*, "Controlling Excited-State Contamination in Nucleon Matrix Elements," Phys. Rev. D **93**, no. 11, 114506 (2016).

[48] B. L. Ioffe, "Space-time picture of photon and neutrino scattering and electroproduction cross-section asymptotics," Phys. Lett. **30B**, 123 (1969).

[49] W. Moris, Y. Q. Ma, J. W. Qiu, A. V. Radyushkin, [In preparation].

[50] R. Edwards, B. Joó, K. Orginos, D. Richards, and F. Winter "U.S. 2+1 flavor clover lattice generation program," Unpublished (2016).

[51] C. G. Boyd, B. Grinstein and R. F. Lebed, "Constraints on form-factors for exclusive semileptonic heavy to light meson decays," Phys. Rev. Lett. **74**, 4603 (1995).

[52] C. Bourrely, I. Caprini and L. Lellouch, "Model-independent description of $B \to \pi l \nu$ decays and a determination of $|V(ub)|$," Phys. Rev. D **79**, 013008 (2009) Erratum: [Phys. Rev. D **82**, 099902 (2010)].

[53] R. A. Briceño, J. V. Guerrero, M. T. Hansen and C. J. Monahan, "Finite-volume effects due to spatially nonlocal operators," Phys. Rev. D **98**, no. 1, 014511 (2018).

[54] B. Joó, J. Karpie, K. Orginos, A. V. Radyushkin, D. G. Richards, R. S. Sufian and S. Zafeiropoulos, "Pion Valence Structure from Ioffe Time Pseudo-Distributions," Phys. Rev. D **99**, no. 11, 114512 (2019).

[55] Rene Brun and Fons Rademakers, "ROOT - An Object Oriented Data Analysis Framework," Proceedings AIHENP'96 Workshop, Lausanne, Sep. 1996, Nucl. Inst. & Meth. in Phys. Res. A 389 (1997) 81-86.

[56] A. Buckley, J. Ferrando, S. Lloyd, K. Nordström, B. Page, M. Rüfenacht, M. Schönherr and G. Watt, "LHAPDF6: parton density access in the LHC precision era," Eur. Phys. J. C **75**, 132 (2015).

[57] G. F. Sterman, "Summation of Large Corrections to Short Distance Hadronic Cross-Sections," Nucl. Phys. B **281**, 310 (1987).

[58] S. Catani and L. Trentadue, "Resummation of the QCD Perturbative Series for Hard Processes," Nucl. Phys. B **327**, 323 (1989).

[59] L. Chang, C. Mezrag, H. Moutarde, C. D. Roberts, J. RodrÃguez-Quintero and P. C. Tandy, "Basic features of the pion valence-quark distribution function," Phys. Lett. B **737**, 23 (2014).

[60] J. H. Zhang, J. W. Chen, L. Jin, H. W. Lin, A. Schäfer and Y. Zhao, "First direct lattice-QCD calculation of the x-dependence of the pion parton distribution function," Phys. Rev. D **100**, 034505 (2019).

[61] J. Towns et al., "XSEDE: Accelerating Scientific Discovery," Computing in Science & Engineering, vol. 16, no. 5, pp. 62-74, Sept.-Oct. 2014.

[62] R. G. Edwards *et al.* [SciDAC and LHPC and UKQCD Collaborations], "The Chroma software system for lattice QCD," Nucl. Phys. Proc. Suppl. **140**, 832 (2005).

[63] M. A. Clark, R. Babich, K. Barros, R. C. Brower and C. Rebbi, "Solving Lattice QCD systems of equations using mixed precision solvers on GPUs," Comput. Phys. Commun. **181**, 1517 (2010).

[64] R. Babich, M. A. Clark and B. Joo, "Parallelizing the QUDA Library for Multi-GPU Calculations in Lattice Quantum Chromodynamics," `arXiv:1011.0024 [hep-lat]`.

[65] B. Joó, D. D. Kalamkar, T. Kurth, K. Vaidyanathan, A. Walden, "Optimizing Wilson-Dirac Operator and Linear Solvers for Intel® KNL" 2016. ISC: High Performance Computing, pp 415-427 30.